Fully CMOS Power Management Unit for Organic Photovoltaic Cells

Sérgio Martins Maciel Moreira (ist192395)
Instituto Superior Técnico
Lisbon, Portugal
sergiommoreira@tecnico.ulisboa.pt

***Abstract*—This paper presents a fully CMOS solution for DC-DC conversion of an organic photovoltaic cell voltage to a standard regulated 1.2V, based on a hard switch boost converter at discontinuous conduction mode (DCM), and a control methodology using a variable frequency LC oscillator (1.2GHz).**

***Index Terms*—Ultra-low power, Power management, boost converter, CMOS, Energy Harvesting.**

I. Introduction

A significant evolution of self-sustained electrical circuits is ongoing for energy harvesting (EH) applications, specially due to the expected increase in the IoT applications. The changing of batteries in this type of systems is expensive [1] and eventually causes environmental issues. Solar cells' availability with reasonable efficiency in indoor environments and the thermoelectric generators are already tested solutions in network sensors or biomedical applications [2].

Forecasts for this type of systems indicates that the number of devices will double between 2018 and 2023, which will result in a necessity to power millions of sensors. The energy harvesters are used in many ways and applications in different environments with the advantage of low maintenance and battery exchanges. Therefore, the energy harvesting supplies' usage brings additional circuits and power management units development [3].

The advance of integrated circuits technology, namely CMOS, contributes to a constant reduction of the electronic circuits dimensions and its power consumption for identical usages [4].

The need for inductive or capacitive step-up converters appears as a solution to convert the energy harvesting low voltage source (typically around hundreds of millivolts) to nominal values such as 1.2V, 2.4V, etc [5], to supply IoT sensors.

Sometimes, the batteries' replacement for specific equipments, such as monitoring sensors for biomedical parameters or data acquisition systems, for different areas of study or leisure, is not that simple, once its localization can restrict the access to the device, for example, in medical devices for human body implant purposes.

New self-sustained energy harvesting solution are studied to increase the autonomy of the electric equipment, of which can be highlighted the vibration (kinetic energy), temperature (thermal energy), radiation (radiofrequency), or from the sun (solar energy) [6], [7], [8], [5].

Emissions of polluting or greenhouse gases produced by these energy sources are null, as are the costs of obtaining energy, both of which are the main reasons why renewable energies are increasingly used. Another added value for this type of energy harvesting source is the portability and the increase in the service life of the energy systems, since the life cycle of the batteries is postponed.

The new solutions for everyday applications with wearables through flexible solar cells in conjunction with ultra-thin batteries are the basis of the motivation for technological advancement in this area [9].

The accomplishment of this work seeks to overcome the constraints of the maximum current limitation imposed by the organic photovoltaic cells, which is expected to be significantly low, the dimensions of the circuit since a reduced implementation area is intended at the outer limits of the active area of OPV and a fully integrated system capable of feeding an IoT sensor.

II. Power Management Unit

The objective of this work is to implement an ultra-low voltage PMU, figure 1, with an organic photovoltaic cell as the energy source. This section shows the proposals and solutions leading to implementing a fully CMOS integrated system, including the control methodology, to regulate the DC-DC converter output to a standard 1.2V voltage.

The proposed architecture shown in figure 1 is prone to be fully integrated in a 130nm CMOS process, allowing an implementation with a very small Silicon footprint.

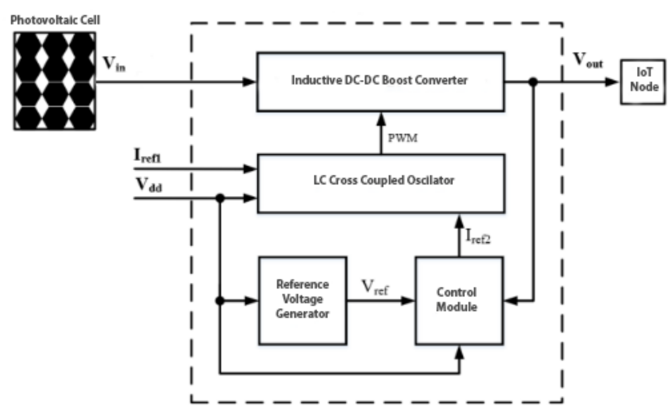

Fig. 1. Block diagram of the proposed PMU.

A. OPV Characterization and modelling

The characterization of the solar cell to be used as energy harvester is necessary to construct and quantify the model to be included in simulations. This characterization was carried out using a Keithley K2400 multimeter/source, a solar simulator Oriel Sol A, 69920, Newport with AM1.5G, in order to simulate solar irradiation on the OPV, a Newport 91150V calibration photovoltaic cell, a four-channel Tektronix TDS3054B oscilloscope, a Voltcraft 7905C multimeter and an Instek GPC-9030DQ power supply.

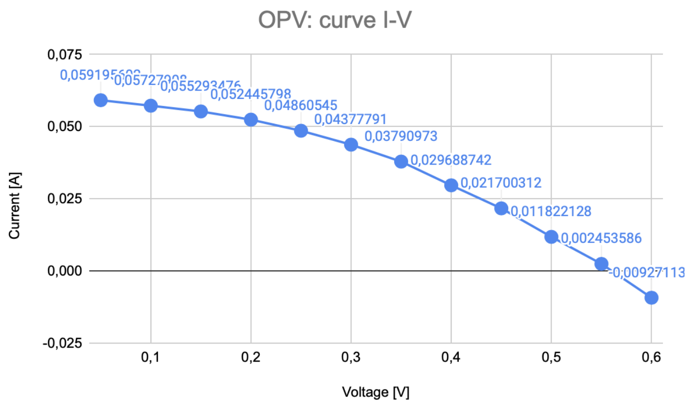

Fig. 2. OPV's I-V curve.

The organic cell from figure 3 is a flexible OPV, with a open circuit voltage of 0.55V and a short circuit current of 61mA.

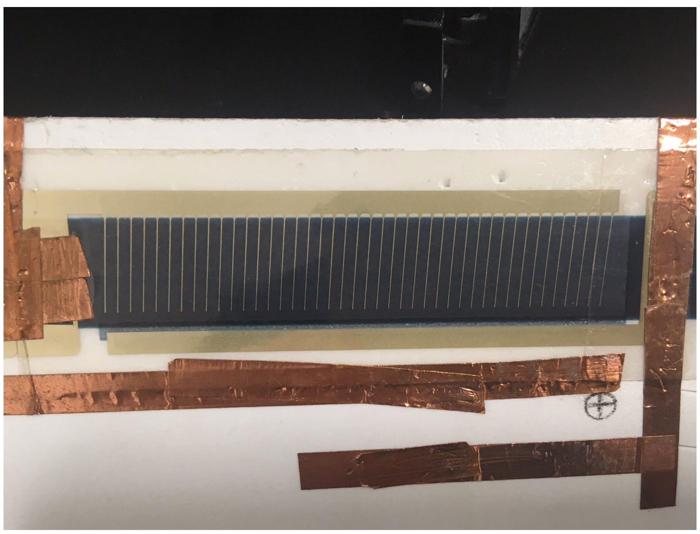

Fig. 3. Organic cell under test.

B. The boost Converter

In order to design the boost converter, it will be necessary to determine the nominal values and dimensions of the four conventional components, namely the inductance value of the L coil, the dimensions and operating parameters of the switch $Q1$ and the diode $D1$, implemented with MOS transistors, and the C filtering capacitor. The circuit used is found in figure 4. This subsection will show some preliminary simulations for validating the switching topology under study.

For the NMOS transistor, given that the circuit to be studied is for ultra-low voltage, it is vital that the transistor has a very low threshold (V_{th}) voltage, ideally zero. Thus, since the MOS has the function of charging the coil by connecting it to earth,

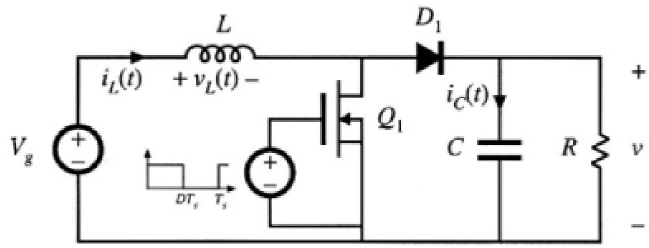

Fig. 4. Hard-switch boost converter [10]

.

TABLE I
DC-DC CONVERT PARAMETERS.

Components	Values
L	$10nH$
Q1 (W/L)	$75\mu m$ / $120nm$
D1 (W/L)	$600nm$ / $2\mu m$
Q2 (W/L)	$300nm$ / $2\mu m$
C	$2.45pF$

the NMOS 1.2V Native Vt Device transistor was chosen, with a typical V_{th} of approximately 0.09 [11]. The diode was chosen taken into account its conductivity without compromising Silicon area.

Concerning the filtering capacitor C, its design process will be based on the equation (1). The capacity value should be determined to obtain a classical value of ripple of 1% in the output voltage (V). As for the implementation, a 130 nm CMOS technology MIM capacitor will be used. Since this capacitor's expected value will be high, the adoption of MIM technology over MOM is more convenient. This choice is due to the fact that the capacitors MIM have more capacity per unit area, thus leading to a reduction of the capacitor footprint [12]. Table I resumes the design parameter's obtained for the boost converter specifications in DCM.

$$\Delta v = \frac{V}{2RC} DT_s \tag{1}$$

C. Oscillator

In order to drive the NMOS device some switching solutions were under study. According to the specified switching frequency range (GHz) a cross-coupled type LC oscillator **oscillator** was under evaluation. This circuit outputs a square wave and, simultaneously, provides a control strategy, based on the oscillation frequency tuning through the voltage imposed on the capacitors.

The oscillator was designed to operate with a nominal frequency of 1.2GHz. Through the V_{tune} input the oscillator spans form 1.25GHz to 1.31Ghz (with a maximum of V_{tune} of 0.6V) as shown in figure 6.

D. Control methodology

The output voltage regulation of the boost DC-DC converter was obtained with a control methodology based on a voltage controlled oscillator. Since the converter was designed to switch in DCM, the output voltage is also dependent on the switching frequency. In this case, by adjusting the voltage applied to the varicap capacitor node, it is possible to increase or decrease the oscillation frequency.

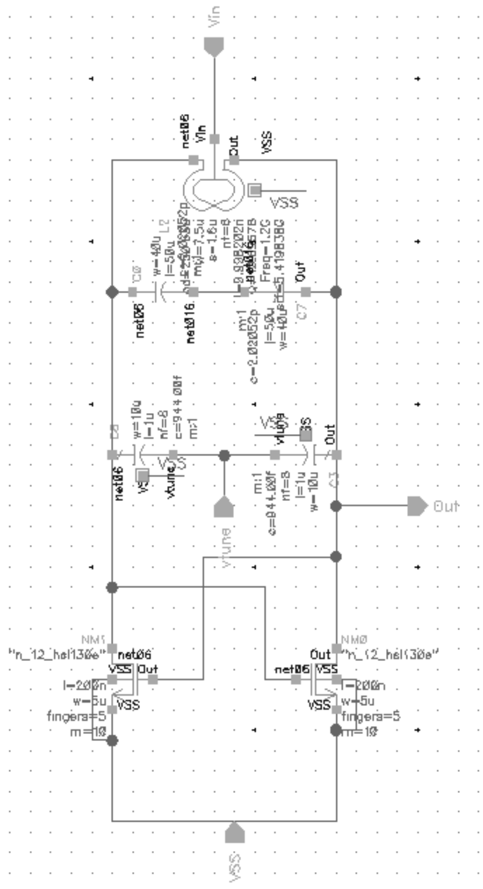

Fig. 5. Cross-coupled LC oscillator used to switch the NMOS device.

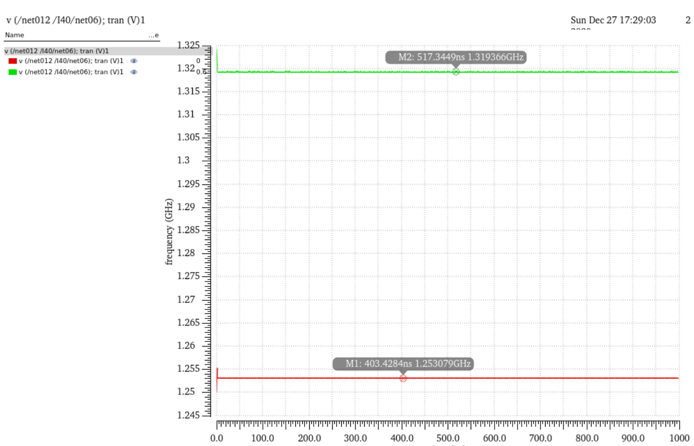

Fig. 6. Maximum (green) and minimum (red) frequency obtained at the oscillator output.

The control implemented consists of comparing a fraction of the output voltage with a reference value to generate a voltage applied to the oscillator's variable capacitor, so that the frequency varies to obtain a regulated conversion ratio.

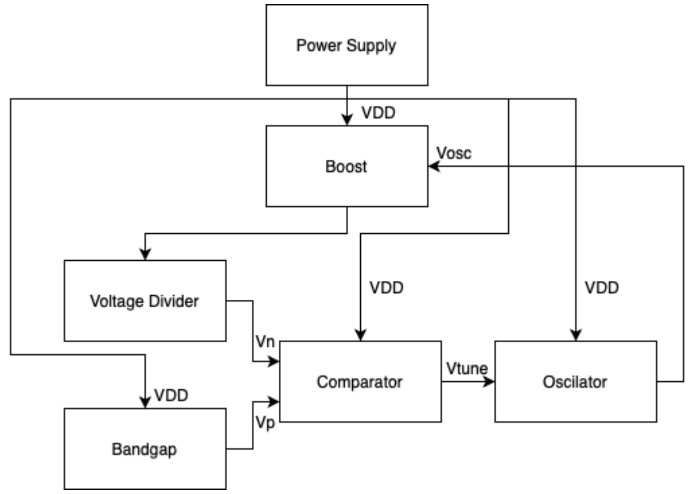

Fig. 7. Block diagram of the control's model.

The block diagram of the converter is shown in figure 7. The control consists of collecting the proportional value of the output voltage through a resistive divider, to be compared with the bandgap's reference value. The oscillator output will then drive the NMOS device with the appropriate frequency in order to achieve a negative feedback loop.

The resistive divider is calculated for the case where the converter reaches 1.2V for a bandgap voltage of 0.165 V, using high-value resistors to reduce consumption but not compromising Silicon area.

Figure 8 represents the operation of the control functional block. Until the converter output reaches 1.2V, the control will be feeding the V_{tune} node of the oscillator with VDD. It is also possible to verify that when the boost reaches 1.2V the control signal (green) is not yet at 0 as theoretically predicted, due to component losses and non idealities of the OPV supply.

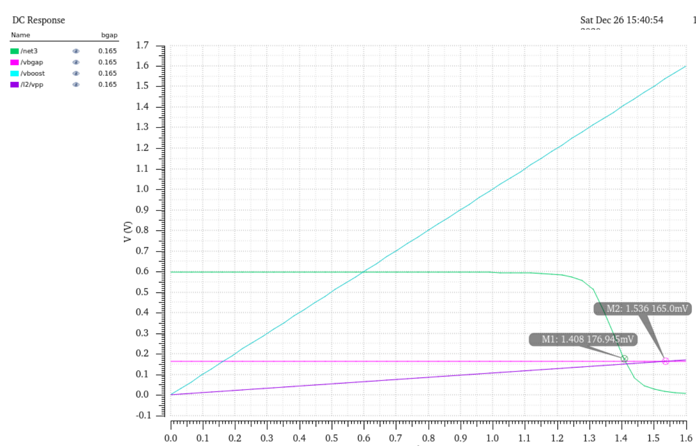

Fig. 8. Functionality of the Controlblock obtained with simulation: input voltage sweep (blue), the comparator/control output signal (green), the reference voltage signal (pink), and the voltage divider output signal (purple).

E. Bandgap

The circuit that is responsible for generating the reference voltage comes from adapting the work done in [13]. The electrical schematic of the circuit is shown in figure 9.

Figure 10 shows simulation results to evaluate the response time of the bandgap reference voltage (165mV). The settling time, less than 1ms, is adequate for the application.

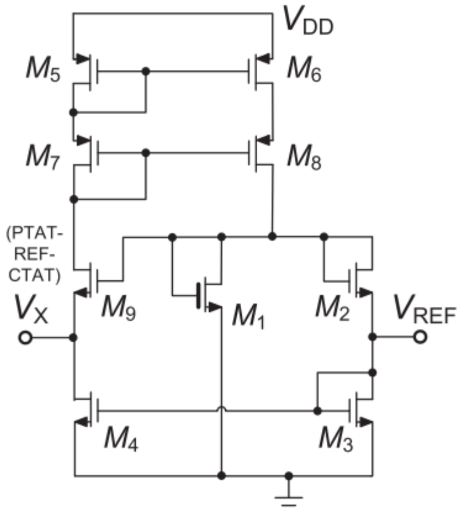

Fig. 9. Schematic of the Bandgap under evaluation [13].

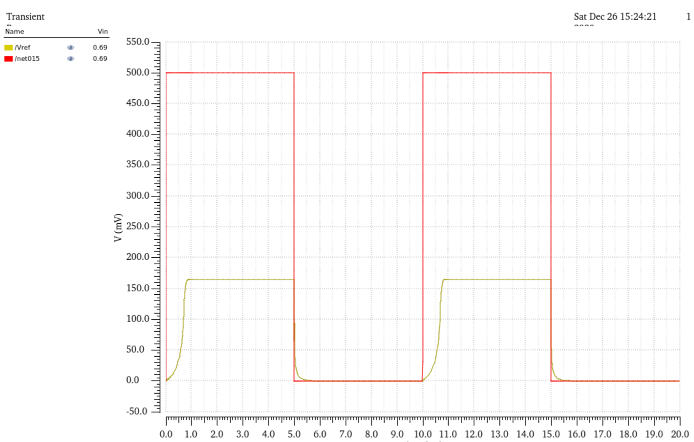

Fig. 10. Bandgap's responde for a square wave type supply.

III. Simulation Results

After the individual validation of each PMU block, they are interconnected and tested in the final system. Table II summarizes the main components and parameters of the various functional blocks of the electronic system.

A. Nominal simulations

The overall PMU testing was started by an evaluation of the load regulation with a scattered input voltage, as shown in figure 14. The lowest output voltage is 1.18V, where it is noticed that the control strategy is no longer working; however, it is possible to see the control's effectiveness in the other simulations. The switching frequency varies between 1.21 and 1.27 GHz, figure 12. It is visible in figure 13 that the signal varies depending on the input voltage. For the lowest input (0.53 V) the boost output is 1.18V, confirming that the contro, signal is laready set to its maximum (red signal). On the other hand, the purple signal (higher output voltage of boost converter) has the control signal at 0 as it already exceeds the desired 1.2 V. Finally, the bandgap signal does not vary significantly with the input voltage, like depicted in figure 14.

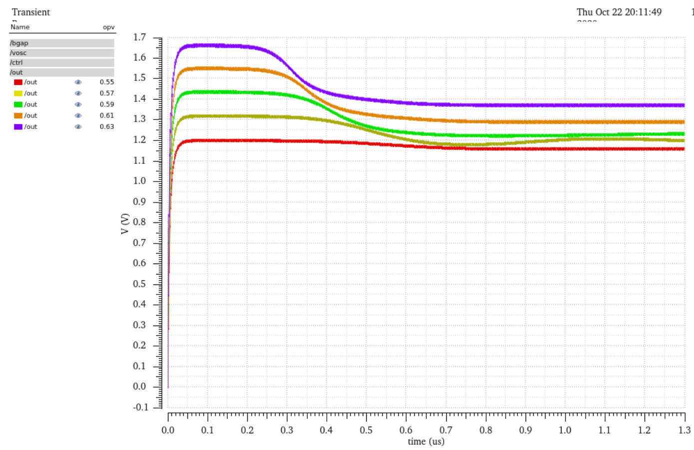

Fig. 11. Output voltage from PMU for different voltage supplies.

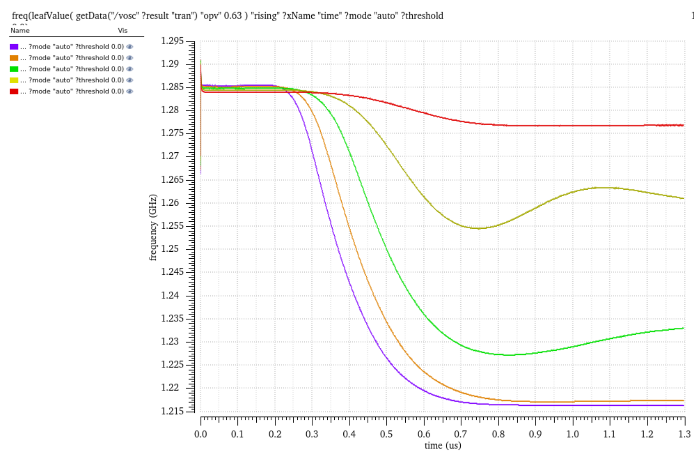

Fig. 12. Oscillator frequency for different voltage supplies.

B. Corners analysis

After the PMU is completely understood, an analysis of corners is performed. The corners analyzed were temperature and transistors dispersion due to process variations. Figure 15 shows that the output voltage for a temperature of 0, 27 and 80 degrees Celsius varies between 1.15V and 1.34V. Once again, the control acts when the voltage is lower than 1.2V and when the circuit alone reaches this value, figure 17. Regarding the frequency, it increases when the control is activated, figure 16. Finally, the bandgap signal fluctuates slightly with temperature, demonstrating that this reference voltage generator is responsible for the converter output voltage dispersion, figure 18.

Four corner process dispersion scenarios were further analysed: fast-fast, fast-slow, slow-fast and finally slow-slow. A variation of 0.3 V was obtained in the boost's output voltage,

TABLE II
TABLE OF GENERAL COMPONENTS AND PARAMETERS.

Boost				
L	**C**	**NMOS (W/L)**	**D (W/L)**	R_L
10 nH	2.45 pF	$75\mu m$ / $120nm$	$600nm$ / $2\mu m$	$45k\Omega$

Oscillator						
L	**C1**	**C2**	**C_var 1**	**C_var 2**	**NMOS 1 (W/L)**	**NMOS 0 (W/L)**
10 nH	2.02 pF	2.02 pF	944 fF	944 fF	$50\mu m$ / $200nm$	$50\mu m$ / $200nm$

Bandgap								
PMOS 0 (W/L)	**PMOS 1 (W/L)**	**PMOS 2 (W/L)**	**PMOS 3 (W/L)**	**NMOS 0 (W/L)**	**NMOS 1 (W/L)**	**NMOS 2 (W/L)**	**NMOS 3 (W/L)**	**NMOS 4 (W/L)**
$22\mu m$ / $19\mu m$	$70\mu m$ / $7\mu m$	$70\mu m$ / $7\mu m$	$22\mu m$ / $19\mu m$	$5\mu m$ / $20\mu m$	$11\mu m$ / $20\mu m$	$11\mu m$ / $19\mu m$	$11\mu m$ / $19\mu m$	$29\mu m$ / $20\mu m$

Control											
R1	**R2**	**R3**	**PMOS 0 (W/L)**	**PMOS 1 (W/L)**	**PMOS 2 (W/L)**	**NMOS 0 (W/L)**	**NMOS 1 (W/L)**	**NMOS 2 (W/L)**	**NMOS 3 (W/L)**	**NMOS 4 (W/L)**
$1M\Omega$	$8.445M\Omega$	$10k\Omega$	$6\mu m$ / $120nm$	$6\mu m$ / $120nm$	$24\mu m$ / $120nm$	$1\mu m$ / $120nm$	$1\mu m$ / $120nm$	$2\mu m$ / $120nm$	$2\mu m$ / $120nm$	$200nm$ / $120nm$

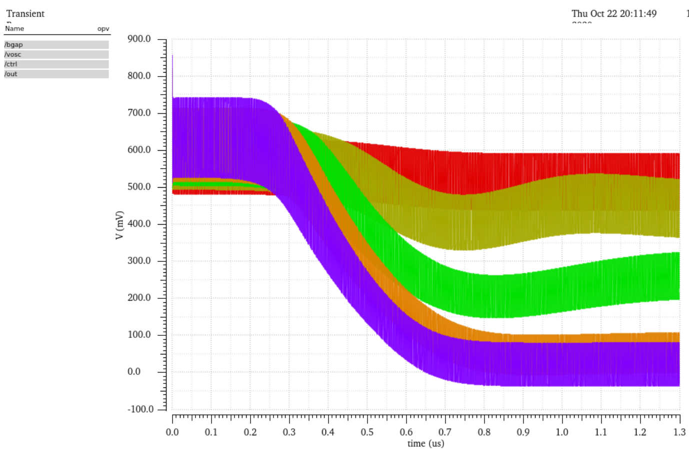

Fig. 13. Control signal for different voltage supplies.

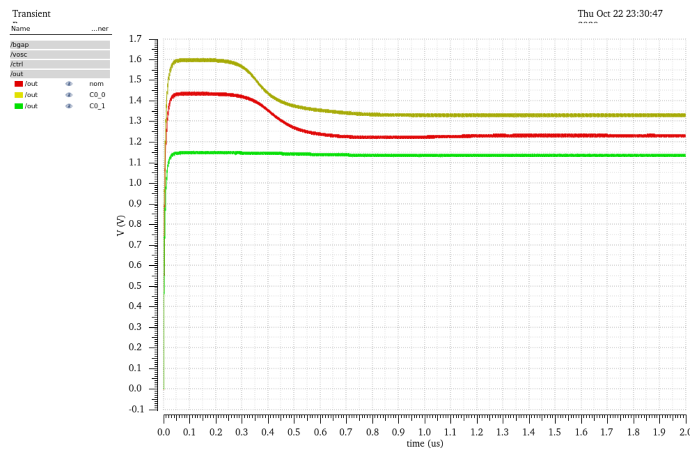

Fig. 15. Output voltage from PMU, temperature corners simulation.

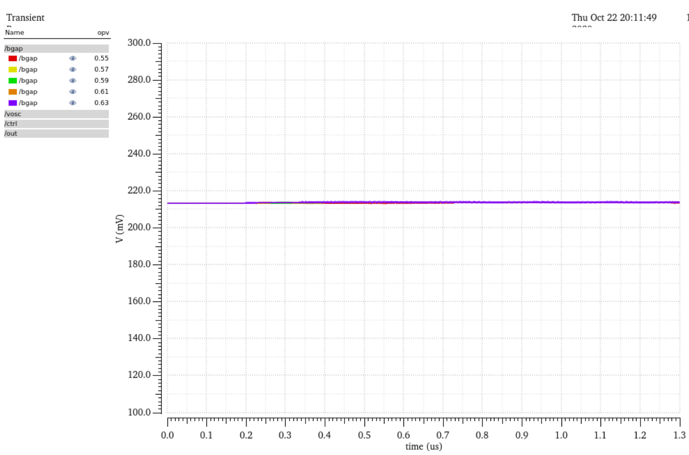

Fig. 14. Bandgap signal for different voltage supplies.

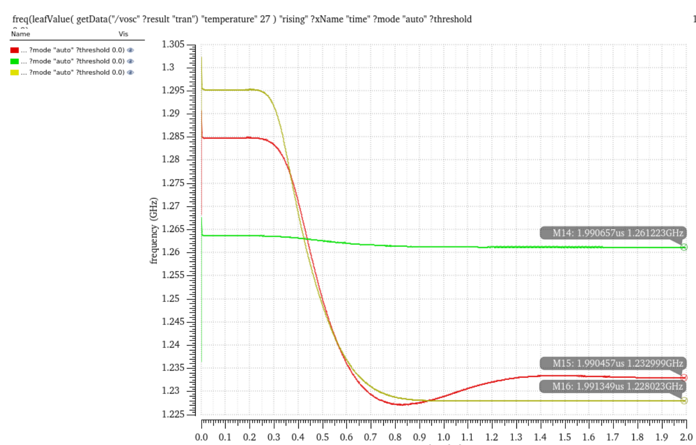

Fig. 16. Oscillator frequency, temperature corners simulation.

the lowest being 1.1V and the highest 1.41V, figure 19. To understand if the converter remains in the expected operating mode, the current in the inductor, figure 20, was also analysed, and it does not undergo significant changes.

Figure 21 shows the oscillation frequency varying from 1.15 GHz to 1.36 GHz, revealing a high sensitivity to the transistors process dispersion. Finally, as previously mentioned, the *bandgap* has some disadvantage , and its generated reference voltage varies significantly, from 100mV up to 300mV.

Finally a layout was made to figure what would be the expected area to be used to produce this circuit, figure 23. The occupied area is $442\mu m^2$.

IV. RELATED WORK

In this section, a review will be done about the various works carried out in energy harvesting to implement voltage step-up circuits based on CMOS technology.

Many of the proposed topologies for switched DC-DC step-up converters are designed for high-power applications, with

TABLE III
STATE OF THE ART COMPARISON

Article	[14]	[15]	[16]	[17]	[18]	[19]	[20]	[21]	PMU
Technology	0.25 μm CMOS	0.35 μm CMOS	0.18 μm CMOS	0.13 μm CMOS	0.18 μm CMOS	0.13 μm CMOS	0.065 μm CMOS	0.13 μm CMOS	0.13 μm CMOS
Topology	*Boost* Inductive	*Boost* Inductive	*Boost* Inductive	*Boost* Inductive	*Boost* Inductive	*Boost* Inductive	*Boost* Inductive	*Boost* Inductive	*Boost* Inductive
Year	2011	2012	2012	2014	2014	2014	2017	2019	2020
V_{in} (V)	0.5 2	0.03 (Start@0.3)	0.12	0.021	0.3	0.6	0.007 (Start@0.21)	0.6	0.5
V_{out} (V)	0 5	1.8	1.2	1	1.1	1.2	-	1.2	1.2
Area (mm^2)	-	1.7	0.273	1.5	0.63	0.31	2.14	0.6	0.442
Freq. (MHz)	0.1	-	1-5	0.1	10	0.1-0.3	40	4.5	1200

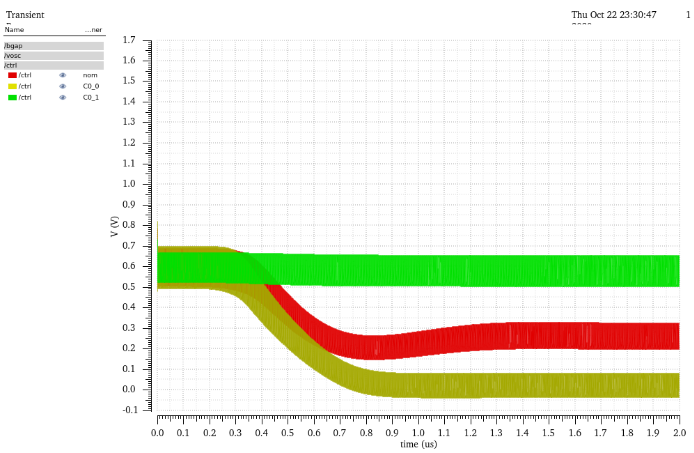

Fig. 17. Control signal, temperature corners simulation.

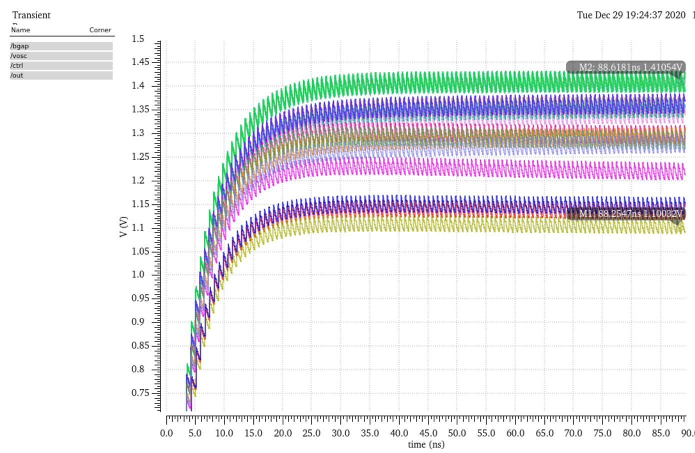

Fig. 19. Output voltage from PMU, transistors corners simulation.

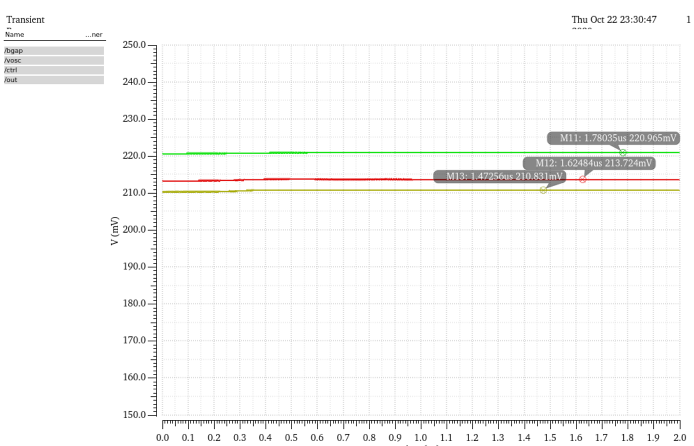

Fig. 18. Bandgap signal, temperature corners simulation.

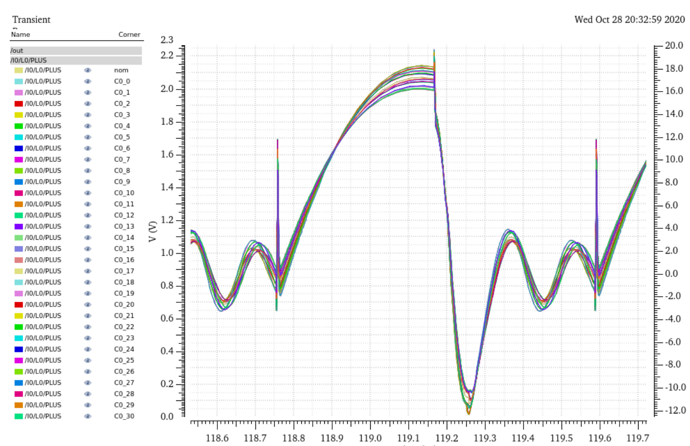

Fig. 20. Oscillator's inductor current, transistors corners simulation.

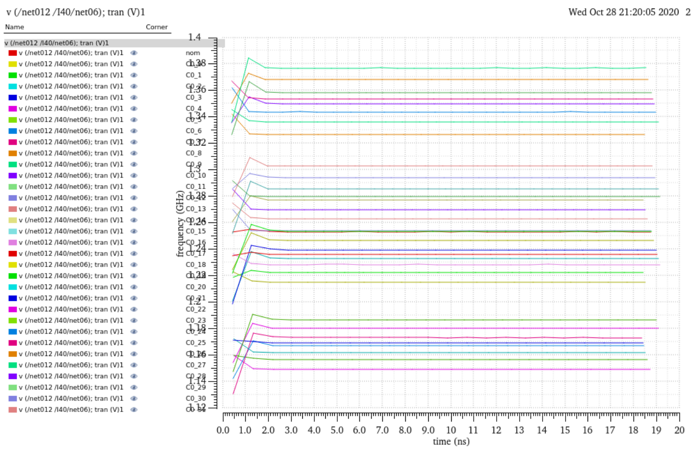

Fig. 21. Oscillator frequency, transistors corners simulation.

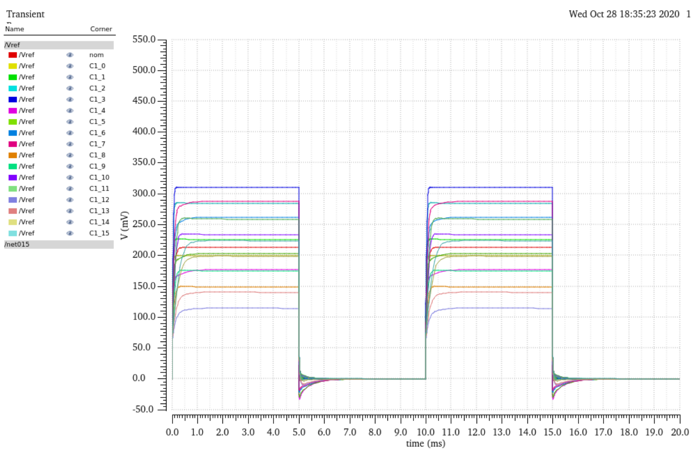

Fig. 22. Bandgap signal, transistors corners simulation.

a relevant conversion coefficient and not always with a small number of devices.

The circuit present in [17] also uses an inductive boost converter. However, it uses a small 1:1 transformer to minimize parasitic capacities, avoiding the effect of multiplying the transformation impedance caused by transformers with a high transformation ratio. The proposed circuit requires a starting voltage of 21 mV, an input voltage of at most 1V, for a regulated output voltage of 1V.

The circuit shown in [18] uses a boost converter with a fully integrated coil in CMOS technology of 0.18 μm. It has an initialization voltage of 300 mV for an output voltage of 1.1V.

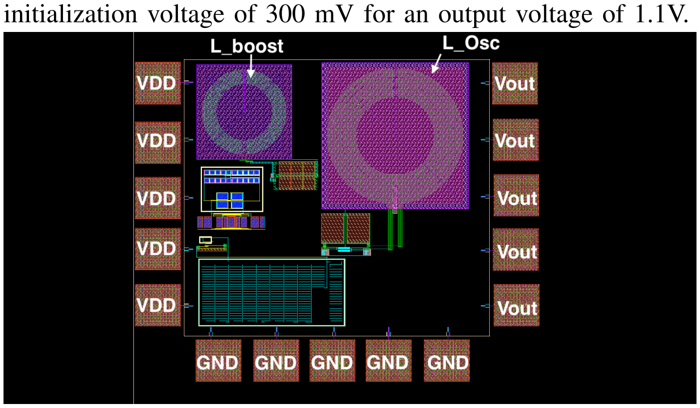

Fig. 23. Full circuit layout.

In [19] it is explained the development of a solution for energy harvesting using a-Si: H cells as energy obtaining devices. The focus of this work is on obtaining energy from lighting conditions indoor. The system presented is based on a DC-DC boost converter that doubles the voltage-controlled from an MPPT algorithm. The energy storage is in charge of a supercapacitor. The great niche of this work is the fact that it works in shallow lighting conditions.

Regarding the circuit present in [20], an inductive boost with an oscillator, a charge pump is used as a secondary start circuit with a voltage of 210 mV and a start voltage of 7 mV. At the output of the circuit, an LDO and a bandgap are proposed in cascade.

Finally, in the circuit in [21], an inductive boost converter with an external 1.2V starting voltage is used. This circuit is not fully integrated as it has an external 47 μH SMD coil. The circuit is tested for meagre power, with an input voltage of 0.6mV obtaining an output voltage of 1.2V.

In order to increase the applicability in the scope of PMU's with origin in energy harvesting, the PMU dimensioned is a fully integrated solution, without recourse external SMD coils. Another aspect developed is the control of the converter with a view to regulating the output voltage. As such, it is in the best interest that the regulated output voltage is obtained without the use of auxiliary or starting supplies. Also it is notable from the table III that there are no circuits reaching this frequency.

V. Conclusions

We present a power management unit, fully integrated, exclusively supplied from an OPV, using 130nm CMOS technology. The designed system includes a boost DC-DC converter, a voltage controlled oscillator with a cross-pair to drive the NMOS switch, and a control block that ensures the output regulation of the power management unit. The circuit is used to increase the output voltage of the OPV which is expected to be non-constant and low (in the order of hundreds of mV) to a standard voltage of 1.2V. After the power management unit's final implementation, it can concluded that the control strategy is adequate and efficient, but further work must be done in order to improve the bandgap corner dispersion.

References

[1] Y. K. Teh and P. K. Mok, "Design consideration of recent advanced low-voltage CMOS boost converter for energy harvesting," *2015 European Conference on Circuit Theory and Design, ECCTD 2015*, no. 21 mV, pp. 1–4, 2015.

[2] M. B. Machado, F. Nornberg, M. Sawan, C. Galup-Montoro, and M. C. Schneider, "Analysis and design of the Dickson charge pump for sub-50 mV energy harvesting," *Microelectronics Journal*, vol. 90, pp. 253–259, 2019.

[3] D. Newell and M. Duffy, *Review of Power Conversion and Energy Management for Low-Power, Low-Voltage Energy Harvesting Powered Wireless Sensors*, Oct. 2019.

[4] M. Gul, Y. Kotak, and T. Muneer, *Review on recent trend of solar photovoltaic technology*, 4. 2016, vol. 34, pp. 485–526.

[5] P. Poure, S. Weber, B. Vidales, M. Madrigal, and D. Torres, "High step-up DC-DC converter for renewable energy harvesting applications," *EEEIC 2016 - International Conference on Environment and Electrical Engineering*, 2016.

[6] S. Chalasani and J. M. Conrad, "A survey of energy harvesting sources for embedded systems," *Conference Proceedings - IEEE SOUTHEASTCON*, pp. 442–447, 2008.

[7] S. B. Huang, J. G. Chen, F. Yang, and Y. H. Cheng, “Design of an ultralow-power CMOS relaxation oscillator for piezoresistive pressure sensor,” *ICSICT 2012 - 2012 IEEE 11th International Conference on Solid-State and Integrated Circuit Technology, Proceedings*, pp. 1–3, 2012.

[8] R. J. Vullers, R. van Schaijk, I. Doms, C. Van Hoof, and R. Mertens, “Micropower energy harvesting,” *Solid-State Electronics*, vol. 53, no. 7, pp. 684–693, 2009. [Online]. Available: http://dx.doi.org/10.1016/j.sse.2008.12.011.

[9] M. Shim, J. Jeong, J. Maeng, I. Park, and C. Kim, “Fully Integrated Low-Power Energy Harvesting System with Simplified Ripple Correlation Control for System-on-a-Chip Applications,” *IEEE Transactions on Power Electronics*, vol. 34, no. 5, pp. 4353–4361, May 2019.

[10] J. Anderson, *Fundamentals of Power Electronics*. 2013, vol. 5, pp. 447–469. [Online]. Available: https://www.crcpress.com/Fundamentals-of-Picoscience/Sattler/p/book/9781466505094#googlePreviewContainer.

[11] UMC, “0.13 um Mixed-Mode and RFCMOS 1P8M Metal Metal Capacitor FSG Enhancement Process Electrical Design Rule,” pp. 1–28, 2006.

[12] ——, “UMC 130nm Metal Metal Capacitor MIMCAPS RF SPICE Model Table of Contents,” pp. 1–16, 2010.

[13] H. Aminzadeh, “All–MOS self-powered subthreshold voltage reference with enhanced line regulation,” *AEU - International Journal of Electronics and Communications*, vol. 122, p. 153 245, 2020. [Online]. Available: https://doi.org/10.1016/j.aeue.2020.153245.

[14] Y. Qiu, C. Van Liempd, B. O. Het Veld, P. G. Blanken, and C. Van Hoof, “5μW-to-10mW input power range inductive boost converter for indoor photovoltaic energy harvesting with integrated maximum power point tracking algorithm,” *Digest of Technical Papers - IEEE International Solid-State Circuits Conference*, no. June 2007, pp. 118–119, 2011.

[15] Q. Liu, X. Wu, M. Zhao, L. Wang, and X. Shen, “30-300mV input, ultra-low power, self-startup DC-DC boost converter for energy harvesting system,” *IEEE Asia-Pacific Conference on Circuits and Systems, Proceedings, APCCAS*, no. 60906012, pp. 432–435, 2012.

[16] A. Richelli, S. Comensoli, and Z. M. Kovács-Vajna, “A DC/DC boosting technique and power management for ultralow-voltage energy harvesting applications,” *IEEE Transactions on Industrial Electronics*, vol. 59, no. 6, pp. 2701–2708, 2012.

[17] Y. K. Teh and P. K. Mok, “Design of transformer-based boost converter for high internal resistance energy harvesting sources with 21 mv self-startup voltage and 74% power efficiency,” *IEEE Journal of Solid-State Circuits*, vol. 49, no. 11, pp. 2694–2704, 2014.

[18] H. Hernández and W. Van Noije, “Fully integrated boost converter for thermoelectric energy harvesting in 180 nm CMOS,” *Analog Integrated Circuits and Signal Processing*, vol. 82, no. 1, pp. 17–23, 2014.

[19] C. Carvalho, G. Lavareda, A. Amaral, C. N. De Carvalho, and N. Paulino, “A CMOS micro power switched-capacitor DC-DC step-up converter for indoor light energy harvesting applications,” *Analog Integrated Circuits and Signal Processing*, vol. 78, no. 2, pp. 333–351, 2014.

[20] Z. Luo, L. Zeng, B. Lau, Y. Lian, and C.-H. Heng, “A Sub-10 mV Power Converter With Fully Integrated Self-Start, MPPT, and ZCS Control for Thermoelectric Energy Harvesting,” *IEEE Transactions on Circuits and Systems I: Regular Papers*, 2017.

[21] D. Batista, L. Oliveira, and P. M. Dos Santos, “Characterization and optimization of an inductive DC-DC converter for ultra-low power energy harvesting,” *Proceedings - 2019 International Young Engineers Forum, YEF-ECE 2019*, pp. 77–82, 2019.